East European Journal of Physics. 4. 125-135 (2022)
DOI:10.26565/2312-4334-2022-4-12 ISSN 2312-4334

NUMERICAL STUDY OF 25.459% ALLOYED INORGANIC LEAD-FREE PEROVSKITE $CsSnGeI_3$-BASED SOLAR CELL BY DEVICE SIMULATION†

Muhammed O. Abdulmalik[a], Eli Danladi[b,*], Rita C. Obasi[c], Philibus M. Gyuk[d], Francis U. Salifu[a], Suleiman Magaji[e], Anselem C. Egbugha[f], Daniel Thomas[d]

[a]*Department of Physics, Confluence University of Science and Technology, Osara, Kogi State, Nigeria*
[b]*Department of Physics, Federal University of Health Sciences, Otukpo, Benue State, Nigeria*
[c]*Centre for Satellite Technology Development-NASRDA, Abuja, Nigeria*
[d]*Department of Physics, Kaduna State University, Kaduna, Nigeria*
[e]*Department of Electronics and Communications Engineering, Nigerian Defence Academy, Kaduna, Nigeria*
[f]*Operations Unit, Starsight Energy, Nigeria*
**Corresponding Author: danladielibako@gmail.com, tel.: +2348063307256*
Received October 16, 2022; revised November 10, 2022; accepted November 12, 2022

The toxic lead component as well as the expensive and less stable spiro-OMeTAD in perovskite solar cells (PSCs) pose a great deal of hindrance to their commercial viability. Herein, a computational approach towards modeling and simulation of all inorganic cesium tin-germanium triiodide ($CsSnGeI_3$) based perovskite solar cell was proposed and implemented using solar cell capacitance simulator (SCAPS–1D) tool. Aluminium doped zinc oxide (ZnO:Al) and Copper Iodide (CuI) were used as electron and hole transport layers (ETL and HTL) respectively. The initial device without any optimization gave a power conversion efficiency (PCE) of 24.826%, fill factor (FF) of 86.336%, short circuit current density (J_{sc}) of 26.174 mA/cm^2 and open circuit voltage (V_{oc}) of 1.099 V. On varying the aforementioned parameters individually while keeping others constant, the optimal values are 1000 nm for absorber thickness, 10^{14} cm^{-3} for absorber layer defect density, 50 nm for ETL thickness, 10^{17} cm^{-3} for ETL doping concentration and 260 K for temperature. Simulating with these optimized values results to PCE of 25.459%, V_{oc} of 1.145 V, J_{sc} of 25.241 mA/cm^2, and a FF of 88.060%. These results indicate that the $CsSnGeI_3$ is a viable alternative absorbing layer for usage in the design of a high PCE perovskite solar cell device.
Keywords: Perovskite solar cells, SCAPS–1D, $CsSnGeI_3$, hole transport material, electron transport material
PACS: 41.20.Cv; 61.43.Bn; 68.55.ag; 68.55.jd; 73.25.+i; 72.80.Tm; 74.62.Dh; 78.20.Bh

1. INTRODUCTION

Metal halide perovskite solar cells (PSCs) belong to one of the most promising photovoltaic technologies for next-generation solar cells. The PSC works based on the following principles: (i) excitons generation when photon energy is absorbed, (ii) excited electrons being drifted into the conduction band (CB) of the electron transport layer (ETL), (iii) holes transferred into the hole transport layer (HTL), and (iv) holes injection into the back-metal electrode [1].

The high power conversion efficiency exceeding 25% from its original value of 3.8% and simple fabrication process of PSCs have triggered the interest of researchers in the photovoltaic community [2–5]. The remarkable performance of PSCs are attributed to high absorption coefficients, a balanced excitons transport, high charge carrier mobilities, long carrier diffusion lengths, and direct and tunable band gaps [6, 7]. However, the presence of toxic lead in perovskite absorber is considered as one of the significant impediments towards its commercial exploitation. In an attempt to replace lead with other less or non-poisonous materials, researchers have considered other divalent metal cations such as tin (Sn^{2+}) and germanium (Ge^{2+}), which have an oxidation state of +2 with an outer layer properties similar to that of Pb^{2+} [8, 9].

The radius of Sn^{2+} (1.35 Å) which is smaller than that of Pb^{2+} (1.49 Å), has resulted to non-distortion of the perovskite nano crystal structure when it is replaced as a divalent cation in lead-based perovskite absorber [10]. Furthermore, due to its narrow band gap of 1.3 eV, it allows high theoretical PCE value to be obtained [11]. A study by Sabba et al. [12] using $CsSnI_3$, $CsSnI_2Br$, $CsSnIBr_2$ and $CsSnBr_3$ as absorbing materials, an interesting band gap of 1.27 eV with outstanding optoelectronic properties for $CsSnI_3$ was obtained. High PCEs were obtained with the lead-free inorganic absorbing material [13, 14]. But Sn^{2+} oxidizes to Sn^{4+} very easily. Therefore, the Sn-based PSCs are susceptible to degradation under ambient environment and hence their efficiencies are affected. The formation energy of Sn vacancies is very low. The formation energy and the change in oxidation state from Sn^{2+} to Sn^{4+} leads to self-doping and also brings about a p-type metallic behaviour [15]. Another candidate for the replacement of Pb^{2+} as a divalent metal cation is Ge^{2+} which has a smaller ionic radius (0.73 Å) than that of Sn^{2+} and Pb^{2+}. Higher conductivity is shown by Ge-based perovskites as compared to the Pb-based perovskites and Sn-based perovskites. Better conductivity and other optoelectronic properties are expected when Ge-Sn alloy is used as replacement of Pb. Chen et al [16] reported a perovskite absorbing material, $CsSnGeI_3$ by alloying $CsSnI_3$ with Ge (II). The device demonstrated excellent stability in air and it outperformed the $CsSnI_3$ and $CsGeI_3$ pristine counterparts, with a PCE of 7%.

The instability caused by organic compounds in PSC has been a major concern for researchers [17, 18]. The vastly used state-of-art hole transport material (HTM), Spiro-OMeTAD demonstrates hygroscopic nature, tendency to crystalize,

† ***Cite as:*** M.O. Abdulmalik, E. Danladi, R.C. Obasi, P.M. Gyuk, F.U. Salifu, S. Magaji, A.C. Egbugha, and D. Thomas, East Eur. J. Phys. **4**, 125 (2022), https://doi.org/10.26565/2312-4334-2022-4-12

and vulnerability to both moisture and heat, as such must be replaced with a cost-effective and stable HTM having high hole mobility with ease of synthesis [19, 20].

The ETL influences the PCE of PSCs by blocking holes, thereby minimizing the charge carrier recombination from the perovskite active layer and hence, providing the photogenerated electrons a pathway to the electrode [21]. A high performing ETL have attributes of high electrical conductivity and high electron mobility which should be comparable to those of the perovskite layer. The most commonly used ETLs are metal oxides such as TiO_2, ZnO and SnO_2, their electrical properties can be tailored by doping [22]. The impact of Aluminium (Al) on zinc oxide (ZnO) as ETL in PSCs was studied by Alias et al [23]. In their study, only the properties of the ETL and interface were explored and a PCE, up to 17.59% was obtained for 1 mol% Al concentration in ZnO. Several properties of PSCs can be studied to give better performance as such necessitated this research.

In the present work, an inorganic, $CsSnGeI_3$-based PSC was studied by utilizing inorganic HTM (CuI) and inorganic electron transport materials (ZnO:Al). By optimizing various properties like thickness of the perovskite absorbing layer, its defect density, the thickness of the electron transport layer, the doping concentration of the electron transport layer, the back-metal contact and temperature, a PCE of 25.459%, with an open circuit voltage of 1.145 V, a short circuit current density of 25.241 mA/cm^2, and a fill factor of 88.060% were obtained. The present work may be helpful in designing and implementing eco-friendly lead free Sn-Ge-alloyed-based PSCs in the future.

2. THEORETICAL METHODS AND DEVICE STRUCTURE

Device simulation is a powerful tool that gives an insight for understanding the electrical and optical properties of solar cells and ultimately providing useful information for design of photovoltaic devices experimentally. In this study, we used the SCAPS-1D software version 3.3.10 to carry out our simulation. This software is designed to simulate multilayer (up to seven layers) solar cells, in which holes and electrons transport are considered by solving the basic semiconductor equations: the Poisson equation and the continuity equation of both charge carriers (holes and electrons) under steady-state condition.

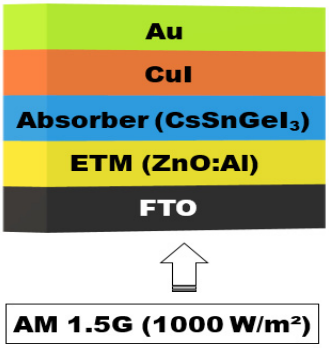

Figure 1. Device structure

This simulation was carried out in the n-i-p configuration of FTO/ZnO:Al/$CsSnGeI_3$/CuI/Au, which is represented in Figure 1. Starting from illumination point, fluorine-doped tin oxide (FTO) is used as a front contact, ETL as ZnO:Al, the absorber layer as $CsSnGeI_3$, HTL as CuI, and gold (Au) as the back metal-electrode. The work function of the front and counter electrode are 4.4 eV and 5.1 eV, respectively. The simulation was done with A.M. 1.5 spectrum (1000 W/m^2) light source, the temperature of the simulation was set at 300 K, the frequency at 1×10^{16} Hz, and a scanning voltage of 0-1.50 V. The details for each layer is as summarized in Table 1. The properties of the defect interface ZnO:Al/$CsSnGeI_3$ and $CsSnGeI_3$/CuI are shown in Table 2.

Table 1. Parameters used for simulation of perovskite solar cell structures using SCAPS-1D [19, 23-26]

Parameters	FTO	ZnO:Al	$CsSnGeI_3$	CuI
Thickness (μm)	0.4	0.22	1.50	0.10
Band gap energy E_g (eV)	3.5	3.25	1.50	2.98
Electron affinity χ (eV)	4.3	4.0	3.9	2.10
Relative permittivity ϵ_r	9	9	28	6.5
Effective conduction band density N_c (cm^{-3})	2.2×10^{18}	2.0×10^{18}	3.1×10^{18}	2.8×10^{19}
Effective valance band density N_v (cm^{-3})	1.8×10^{19}	1.8×10^{19}	3.1×10^{18}	1.0×10^{19}
Electron thermal velocity (cm/s)	1.0×10^{7}	1.0×10^{7}	1.0×10^{7}	1.0×10^{7}
Hole thermal velocity (cm/s)	1.0×10^{7}	1.0×10^{7}	1.0×10^{7}	1.0×10^{7}
Electron mobility μ_n (cm^2 V^{-1} s^{-1})	2.0×10^{1}	3.0×10^{2}	9.74×10^{2}	1.69×10^{-4}
Hole mobility μ_p (cm^2 V^{-1} s^{-1})	1.0×10^{1}	2.5×10^{1}	2.13×10^{2}	1.69×10^{-4}
Donor concentration N_D (cm^{-3})	1.0×10^{18}	7.25×10^{18}	0	0
Acceptor concentration N_A (cm^{-3})	0	0	1×10^{19}	1×10^{18}
Defect density N_t (cm^{-3})	1×10^{15}	1×10^{14}	1×10^{11}	1×10^{12}

Table 2. Defect parameter values of the interfaces of the device

Parameters	$ZnO:Al/CsSnGeI_3$ interface	$CsSnGeI_3/CuI$ interface
Defect type	Neutral	Neutral
Capture cross section for electrons (cm^2)	1×10^{-15}	1×10^{-18}
Capture cross section for holes (cm^2)	1×10^{-15}	1×10^{-16}
Energetic distribution	Single	Single
Energy level with respect to E_v (eV)	0.600	0.600
Characteristic energy (eV)	0.1	0.1
Total density (cm^{-3})	1×10^{11}	1×10^{12}

3. RESULTS AND DISCUSSION

3.1. Performance study of the initial device, quantum efficiency and energy band profile

The current-voltage (*J-V*) characteristics of the initial perovskite solar cell device simulated under illumination is shown in Figure 2(a).

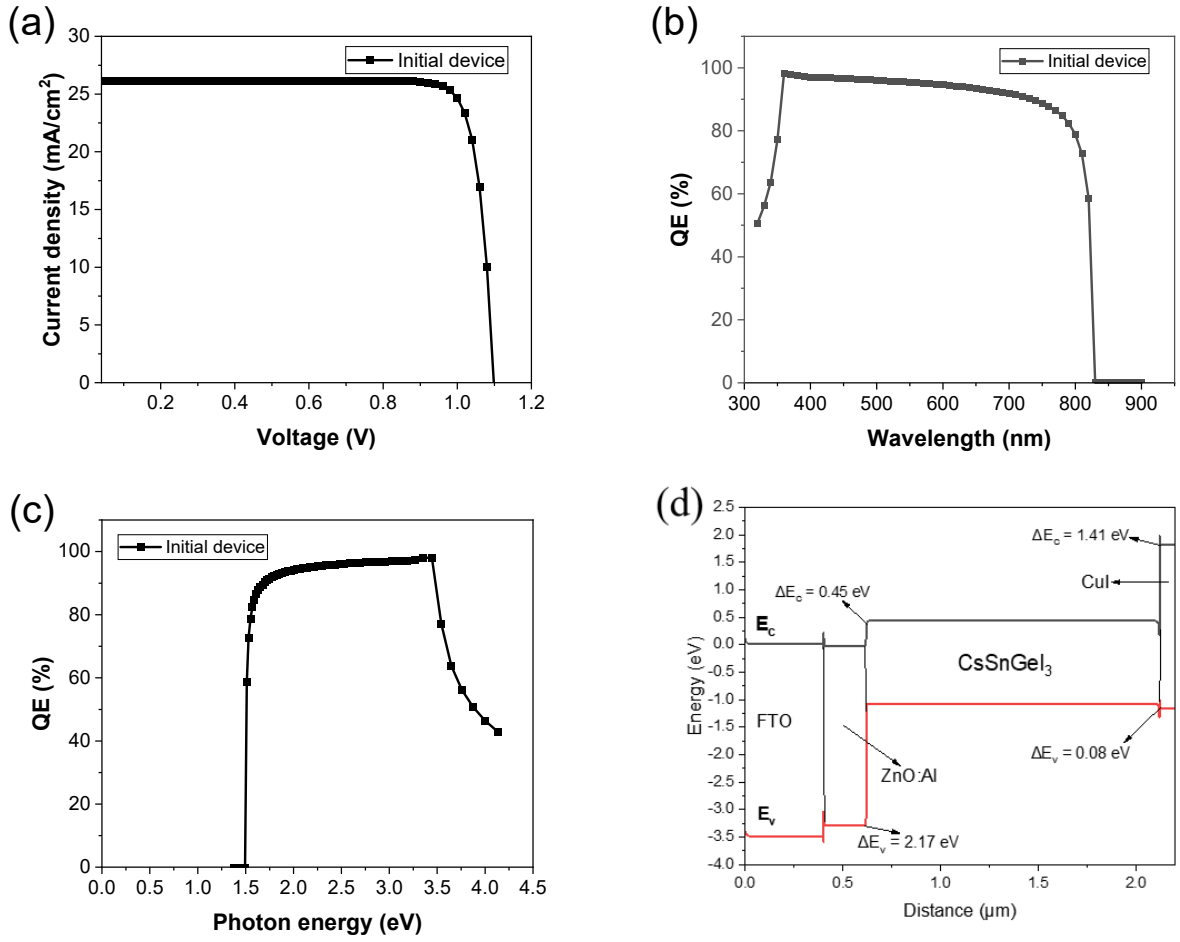

Figure 2. (a) *J-V* curve of PSC with initial solar cell characteristics, (b) quantum efficiency against wavelength, (c) quantum efficiency against photon energy and (d) energy profile band diagram

Under illumination, a V_{oc} of 1.099 V, J_{sc} of 26.174 m/Acm^2, FF of 86.336%, and PCE of 24.826% were obtained. Comparing these solar cell characteristics with simulated work on $CsSnGeI_3$ perovskite obtained by a group of researchers [26], comparable V_{oc} (1.00 V) and J_{sc} (25.75 m/Acm^2) were obtained. In our simulation, we obtained appreciable values of FF, PCE which are higher than those from their simulated research work. This could be attributed to the increase in conductivity of the ETL due to doping and different HTL used. Figure 2b & c shows the quantum efficiency against wavelength and photon energy. It is within the range of 300 to 900 nm, which has maximum attained value of 98% observed at 360 nm. It sweeps across the visible region which satisfies the device's requirement. The strong absorption at the visible region of the QE curve is a factor that determines the light absorption strength at the various wavelengths of light and the cut-off region at 850 nm which certified the band gap of 1.5 eV for $CsSnGeI_3$ [25]. Figure 2d shows the energy band diagram of ETL/perovskite/HTL materials in the device structure, with the interface conduction and valence band offset at the $ZnO:Al/CsSnGeI_3$ interface of 0.45 eV and 2.17 eV while at the $CsSnGeI_3/CuI$ interface,

the interface conduction and valence band offset are 1.41 eV and 0.08 eV respectively. These values are beneficial for flow of charge careers within the interface and subsequently result to enhanced device performance.

3.2. Effect of the absorbing layer thickness

The absorbing layer thickness is one of the important parameters having a significant impact on the device's performance. A good choice of this thickness is very essential to determine better device's performance. In order to study its impact on the perovskite solar cell, the $CsSnGeI_3$ layer thickness was varied in the range of 100–1000 nm while keeping all other parameters untouched as detailed in Tables 1 and 2. The *J-V* curve and the quantum efficiency of the performance with varied device is shown in Figure 3a & b. The effect of the variation of the absorbing layer thickness on the device parameters; V_{oc}, J_{sc}, FF and PCE are shown in Figures 3c & d.

The V_{oc} and J_{sc} rise sharply with corresponding increase in thickness of absorbing layer up to a thickness of 500 nm, and rises steadily from 600 to 1000 nm as shown in Figure 3(d). PCE of the device is low when thickness of the absorbing layer is too small as shown in Figure 3(c), which is evident to poor absorption of light by the material. As the thickness of the absorbing layer increases, the number of photo-generated charge careers increases leading to greater PCE of device, due to more photons being absorbed by the material [27].

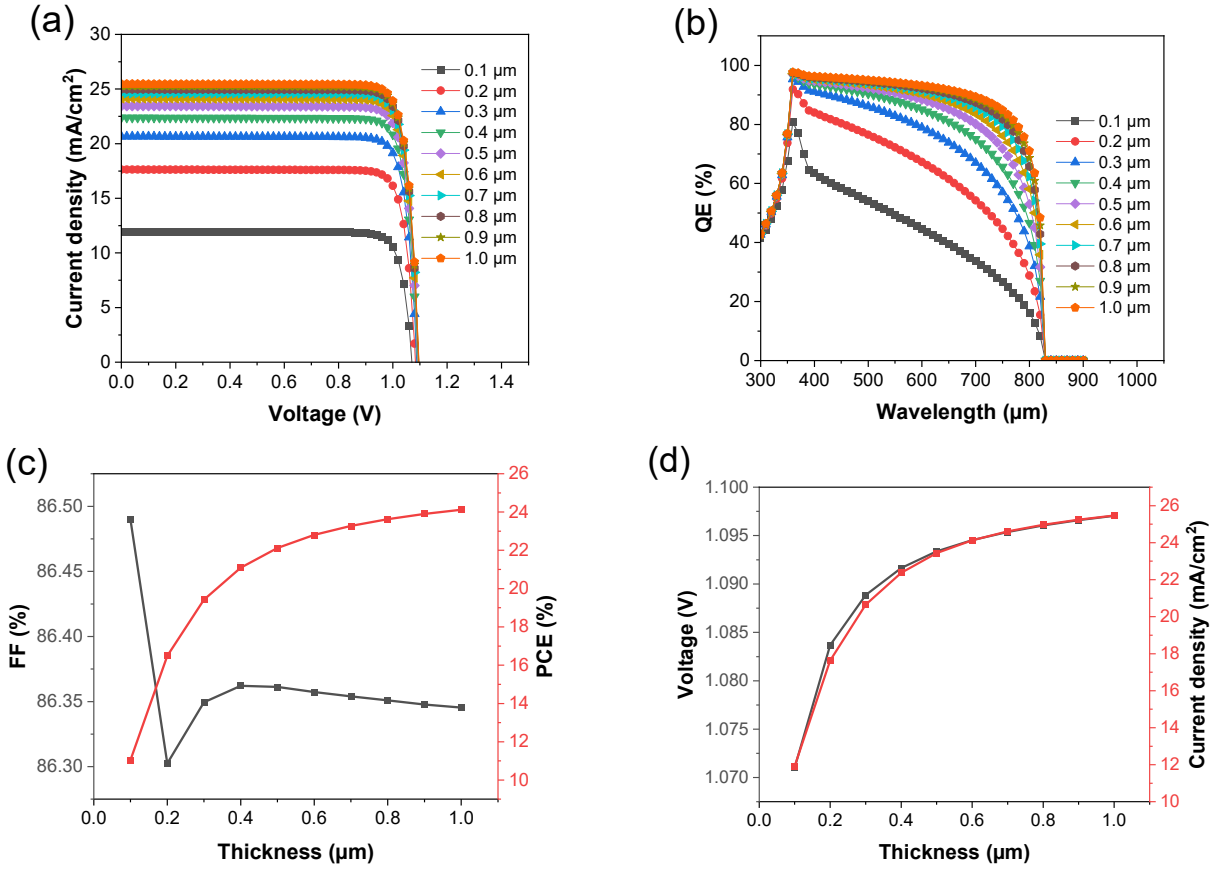

Figure 3. (a) *J-V* curve with varied absorber thickness under illumination, (b) QE curve with respect to wavelength, (c) PCE and FF with respect to thickness and (d) J_{sc} and V_{oc} with respect to varied absorber thickness

The fill factor decreases rapidly from 100 to 200 nm of absorbing layer thickness, before increasing slightly to a peak value of 400 nm of thickness, and finally decreases steadily when the absorbing layer thickness increases beyond 400 nm. The decrease in the value of FF in relation to absorber layer thickness is due to an increase in series resistance [28].

Therefore, the optimal thickness of the $CsSnGeI_3$ in our research work was 1000 nm and as such considered for further simulation. The device performance at that thickness gave the following metric performance: PCE = 24.122%, FF = 86.345%, J_{sc} = 25.466 mA/cm^2, and V_{oc} = 1.097 V.

The quantum efficiency versus wavelength plot for the device with varied thickness is shown in Figure 3b. The QE increases with increasing thickness of $CsSnGeI_3$ from 80% at 100 nm to 99.4% at 1000 nm. The strong QE is due to increase in absorption coefficient as the thickness increases [20].

3.3. Effect of absorbing layer defect density

The surface and bulk of the absorbing layer are prone to defects which are unavoidably present. In perovskite layers, lattice vacancy, interstitial, schottky, and frenkel defects are such defects which can be found as point defects [29]. When PSCs absorb

light, the absorbing layer in turn generates photoelectrons, and if the film quality is poor, there will be an increase in defect density, leading to quenching losses in absorbing layer which is a determining factor for the V_{oc} of the solar cell [19]. From research findings, in lead-free perovskites films, minimal grain boundary length and the carrier recombination occur due to their improved quality crystal grains. Long carrier diffusion length is responsible for decrease in further recombination which is observed in perovskite films with lesser defects [30, 31]. The Shockley-Read-Hall (SRH) recombination model can be used to study the impact of the absorbing layer defect density on the performance of a solar cell [32].

The defect density (N_t) of the absorbing layer was varied from 10^{14} to 10^{19} cm^{-3} and its impact on the device photovoltaic parameters is explored systematically. The *J-V* curve and QE for varied N_t is shown in Figures 4a & b. Figures 4c & d show the correlation between PCE, FF, J_{sc} and V_{oc} with N_t. Increase in defect density of the absorbing layer, results to decrease in the photovoltaic parameters of the cell. This can be attributed to increase in the carrier recombination of the device [19]. From the values of 10^{16} to 10^{17} cm^{-3}, slight decrease was observed across all photovoltaic parameters. From the values of 10^{17} to 10^{18} cm^{-3} of defect density, a sharp decline across all photovoltaic parameters were observed, and finally a drastic fall in the performance of the device from 10^{18} to 10^{19} cm^{-3}. The optimized value of absorbing layer defect density was chosen as 10^{14} cm^{-3} with photovoltaic parameters: V_{oc} of 1.099 V, J_{sc} of 26.213 mA/cm^2, FF of 86.336%, and PCE of 24.866%.

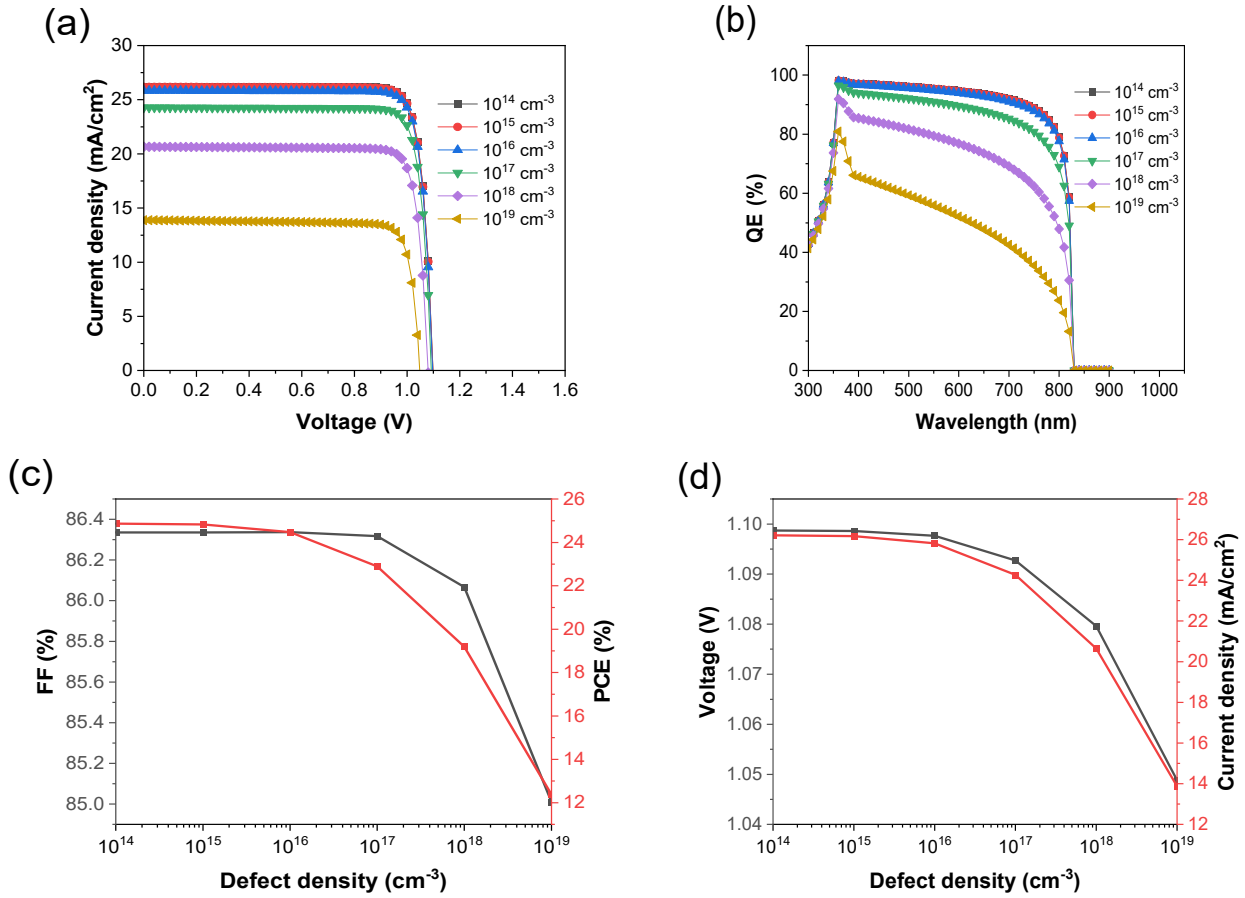

Figure 4. (a) *J-V* curve with varied absorber defect density under illumination, (b) QE curve with respect to wavelength, (c) PCE and FF with respect to absorber defect density and (d) J_{sc} and V_{oc} with respect to varied absorber defect density

3.4. Effect of ETL thickness

The thickness of ETL can greatly affect the performance of solar devices [33]. The function of the ETL is tasked with blocking holes, extraction and transporting the photo-electrons in the absorbing layer and prevention of the charge carrier recombination of holes and electrons in the front electrode in the absorbing layer [34]. This parameter is very important for device optimization in order to enhance the performance of PSCs. The thickness of ETL was varied from 50 to 500 nm and the resulting variation in device photovoltaic parameters is shown in Figures 5a-d. Figures 5a & b show the *J-V* plot and QE curve with varied ETL thickness while Figures 5c & d show the correlation of photovoltaic parameters with ETL thickness. It is observed that as the thickness of ETL increases, the performance of the device for simulated PSCs decreases. Steady decrease was observed through the V_{oc}, J_{sc}, and PCE of the device, as the thickness of the ETL increases. However, the FF increases steadily as there was increment in the ETL thickness. Optimal values were observed at the thickness value of 50 nm with V_{oc} of 1.099 V, J_{sc} of 26.190 mA/cm^2, FF of 86.336%, and PCE of 24.841%. The optimal value was used for further simulation.

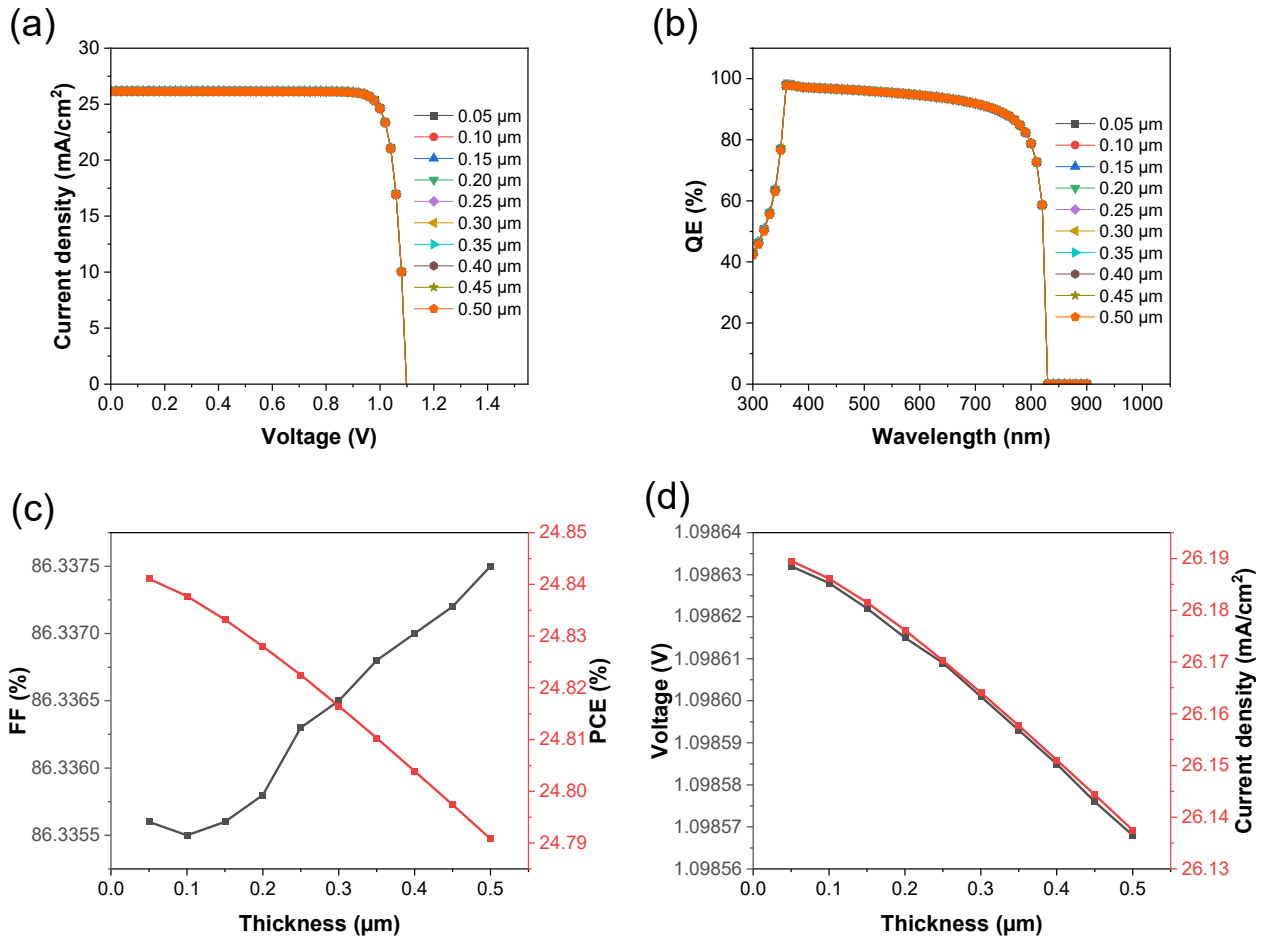

Figure 5. (a) *J-V* curve with varied ETL thickness under illumination, (b) QE curve with respect to wavelength, (c) PCE and FF with respect to ETL thickness and (d) J_{sc} and V_{oc} with respect to varied thickness

The chances of recombination are increased as the thickness of the ETL is increased, for the fact that charges take longer route of travel for diffusion to occur, leading to reduction in the PCE of the device. The efficiency decrease at a certain rate with corresponding increment in the ETL thickness, is apparently due to an increase in recombination [35,36]. Selecting the thickness from 50 to 500 nm results to spectral overlap in the QE versus Wavelength curve which is attributed to unchanged optical absorption efficiency within the selected values of thickness as shown in Figure 5b.

3.5. Effect of ETL doping concentration

Current generation is enhanced as electrons are being accelerated as a result of doping concentration of the ETL. The charge carrier conductivity is enhanced as there is an effective suppression of the ETL/absorber interface defects due to the introduction of n-type Al dopant in the ZnO ETL to replace the Zn^{2+}. The introduction of a donor level at 120 meV below the conduction band can lead to an appropriate band alignment, and an increase in the free carrier concentrations [37].

The doping concentration was varied from 10^{11} to 10^{19} cm^{-3} for the ETL. Figures 6a & b show the *J-V* behaviour and QE properties of the simulated device with varied ETL doping concentration while Figures 6c & d show the variation of performance parameters with doping concentration of ETL. There was a decrease in the V_{oc}, PCE and FF of the device as the doping concentration increased; steady decrease was observed in the V_{oc} before a rapid decrease was observed from 10^{18} to 10^{19} cm^{-3}. The PCE of the device experiences an increase from the values of 10^{15} to 10^{17} cm^{-3}, before following a declining path. The FF of the device experiences an increase from the values of 10^{13} to 10^{16} cm^{-3}, before following a declining path. The J_{sc} of the device experiences an increase from the values of 10^{15} to 10^{17} cm^{-3}. The optimized values of photovoltaic parameters were chosen at a V_{oc} of 1.149 V, J_{sc} of 25.922 mA/cm^2, FF of 88.260%, and PCE of 26.280% for an ETL doping concentration of 10^{17} cm^{-3}. There was spectral overlap at the QE plot which shows an unchanged optical absorption within the selected doping concentration values.

3.6. Effect of back-metal contact work functions on the device

The back-metal contact is deposited over the perovskite absorber or HTM, for holes collection from the external circuit. The formation of an ohmic contact is vital to facilitate proper majority charge carrier collection (holes via the

back-metal contact). The work function of different back-metal contacts was studied to understand their effect on the performance of the device. The back-metal contact work functions studied were; Carbon (C) of 5.00 eV, Gold (Au) of 5.1 eV, Palladium (Pd) of 5.30 eV, and Platinum (Pt) of 5.65 eV.

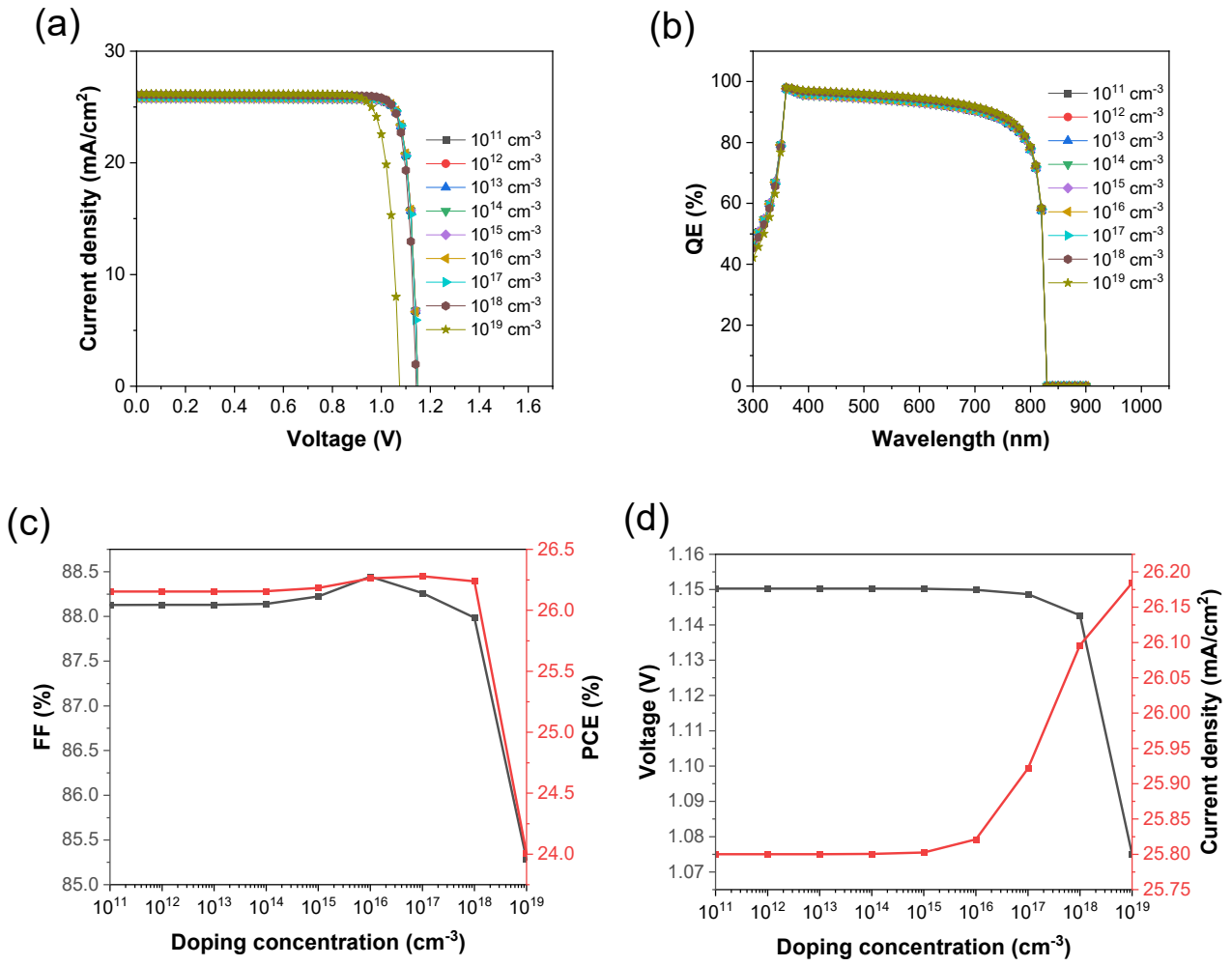

Figure 6. (a) *J-V* curve with varied doping concentration under illumination, (b) QE curve with respect to wavelength, (c) PCE and FF with respect to doping concentration and (d) J_{sc} and V_{oc} with respect to doping concentration

The impact of the back-metal contact work functions on the performance of the device is shown in Figures 7a-d with Figure 7a showing the *J-V* curve, 7b showing the QE and 7c & d showing the performance correlation with metal back contacts. As observed, when the back-metal work functions increased from 5.00 to 5.65 eV, there were no changes observed in the J_{sc} and V_{oc} values. The FF values increased from 86.277 to 86.344%, and PCE from 24.809 to 24.828%.

From the results obtained, it can be seen that, as the back-metal work functions increases, there is efficiency enhancement improving the performance of the device in turn. For this device, it can be concluded that a high PCE can be achieved when the back-metal work function is not less than 5.1 eV. The optimized values of photovoltaic parameters were chosen at a V_{oc} of 1.097 V, J_{sc} of 26.174 mA/cm^2, FF of 86.344%, and PCE of 24.828% for the back-metal contact of Pt with a work function of 5.65 eV for this device. There was spectral overlap at the QE plot which shows an unchanged optical absorption within the selected back-metal contact.

3.7. Effect of temperature on the device

Solar cells are generally installed outdoors, and the temperature will increase due to continuous solar radiation even higher than normal room temperature of 300 K. Therefore, it is necessary to understand the performance of the device with these variations in temperature. The device was varied from an operating temperature of 260 to 350 K subjected to constant illumination. The effect of temperature on the *J-V* curve is shown in Figure 8a. The correlation between the PCE, FF, J_{sc} and V_{oc} with temperature is shown in Figures 8b & c. From observation, as the temperature increases from 260 to 350 K, the V_{oc} decreases linearly from 1.150 to 1.034 V, the FF decreases steadily from 87.926 to 84.093%, and PCE decreases from 25.172 to 23.942%. However, the J_{sc} of the device increases steadily with temperature increase from 24.897 to 27.538 mA/cm^2.

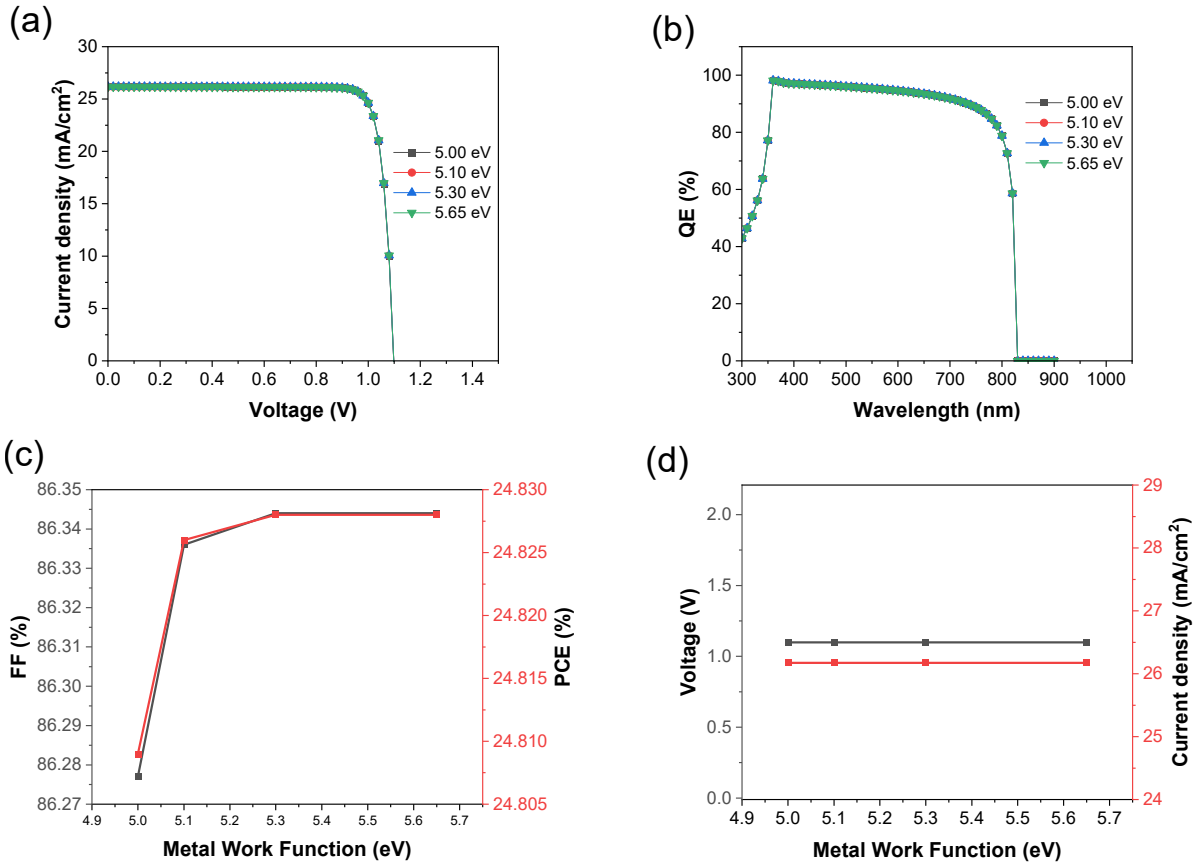

Figure 7. (a) *J-V* curve with different metal contact under illumination, (b) QE curve with respect to wavelength with different metal contact, (c) PCE and FF with respect to metal contact and (d) J_{sc} and V_{oc} with respect to metal contact

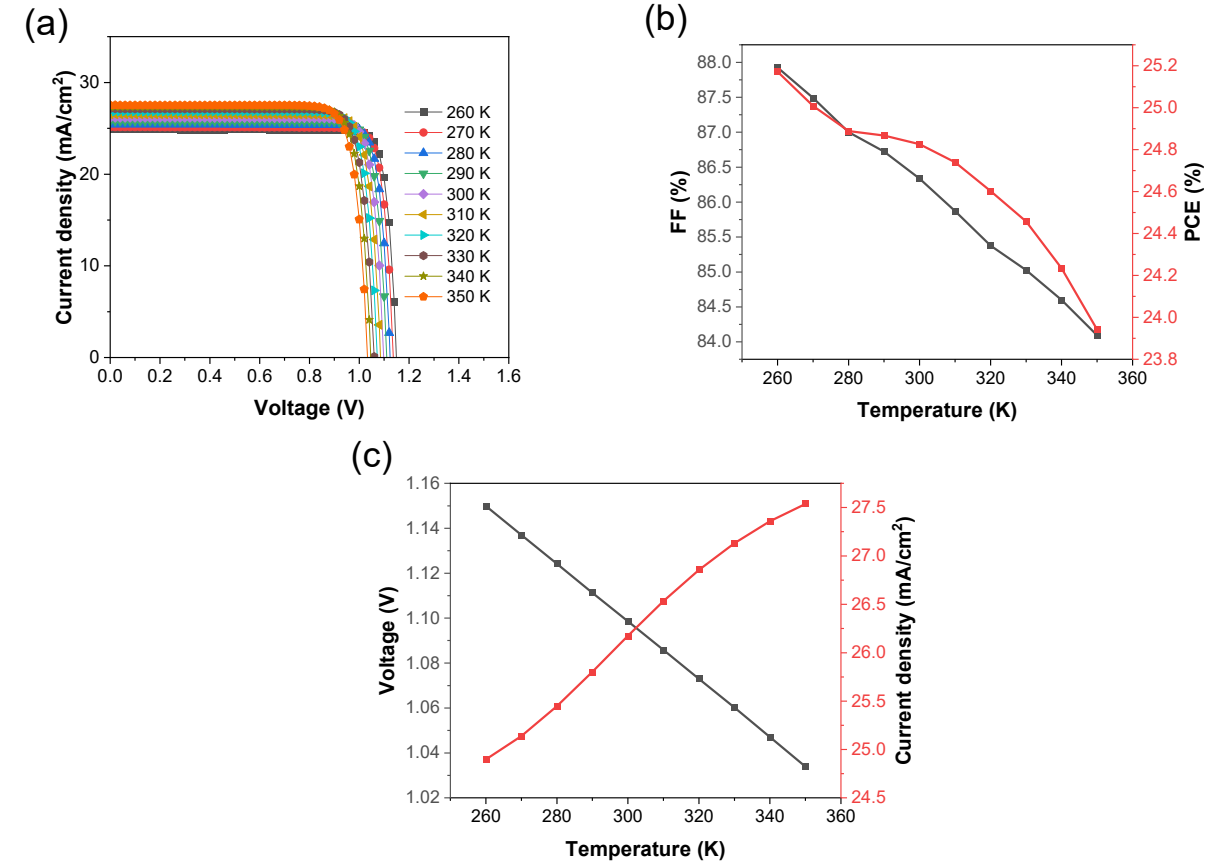

Figure 8. (a) *J-V* curve with varied temperature under illumination, (b) PCE and FF with respect to temperature and (c) J_{sc} and V_{oc} with respect to temperature

The behavior exhibited by the J_{sc} is due to the metastable nature of the device at higher temperatures [38]. The electrons absorb enough photons and hence recombines with positive charge carriers that have been already generated, becoming a site for recombination, leading to an unstable state [38]. The decrease in V_{oc} is attributed to the increase in defects as the temperature of the device increases. Change in the resistance of the device occurs as the temperature increases which affects electron and hole mobilities, and the carrier concentration leading to a decrease in PCE.

3.8 Performance study of the initial and optimized device

The *J-V* characteristics of the initial and optimized perovskite solar cell device simulated under illumination is shown in Figure 9. Under illuminated condition, the performance of the optimal PSC is as follows: $V_{oc} = 1.145$ V, $J_{sc} = 25.241$ mA/cm^2, FF = 88.060% and PCE = 25.459%. Upon comparing with the initial device, an appreciable improvement of ~4.20%, ~2.00% and ~2.56% in V_{oc}, FF and PCE respectively were observed.

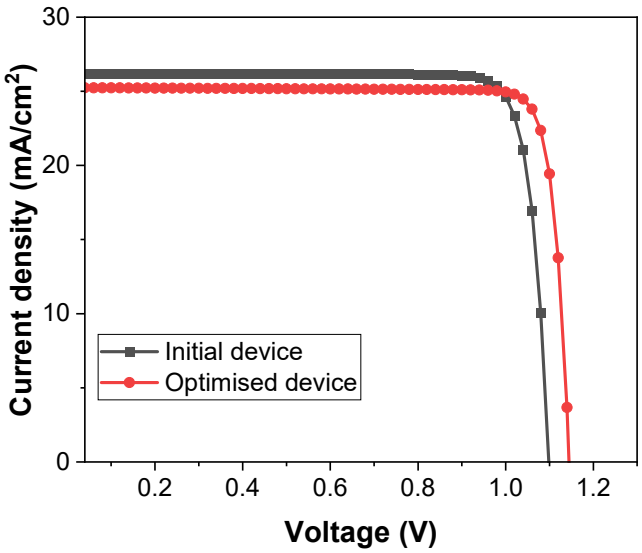

Figure 9. Initial and optimized of *J-V* curves the device

4. Conclusion

In this paper, the numerical investigation of lead-free $CsSnGeI_3$-based perovskite solar cell was performed using SCAPS-1D simulation software. The device performance was studied to achieve better efficiency with respect to (i) effect of the absorbing layer thickness, (ii) effect of absorbing layer defect density, (iii) effect of ETL thickness, (iv) effect of ETL doping concentration, (v) effect of back-metal contact work functions and (vi) effect of temperature on the device. Our study revealed that better photovoltaic parameters were obtained when the optimal values of the absorbing layer thickness was 1000 nm, the absorbing layer defect density was 10^{14} cm^{-3}, the ETL thickness was 50 nm, the ETL doping concentration was 10^{17} cm^{-3} and the best performing back-metal contact was Pt with a work function of 5.65 eV. Also, the $CsSnGeI_3$-based perovskite solar cells are very sensitive to temperature with an optimized value of 260 K. There was significant degradation of PV parameters as the temperature of the device increases, adversely affecting material conductivity. The optimized device (FTO/ZnO:Al/$CsSnGeI_3$/CuI/Pt) gives PCE of 25.459%, V_{oc} of 1.145 V, J_{sc} of 25.241 mA/cm^2, and fill factor of 88.060%. A 2.56% improvement in PCE and 4.20% improvement in V_{oc} were obtained over the initial device. This numerical simulation paves better understanding on the choice of parameters leading to a high performing PSCs, stability enhancement and characterization.

Acknowledgments

The authors would like to thank Professor Marc Burgelman and his team from the Department of Electronics and Information Systems, University of Ghent, Belgium, for the development of the SCAPS software package and allowing its use.

Conflict of interest. Authors have declared that there is no conflict of interest.
Funding. This article did not receive any funding support.

ORCID IDs

Muhammed O. Abdulmalik, https://orcid.org/0000-0002-3250-7864; **Eli Danladi**, https://orcid.org/0000-0001-5109-4690
Francis U. Salifu, https://orcid.org/0000-0001-9015-2347

REFERENCES

[1] S. Ameen, M.A. Rub, S.A. Kosa, K.A. Alamry, M.S. Akhtar, H.S. Shin, H.K. Seo, A.M. Asiri, and M.K. Nazeeruddin. ChemSusChem, **9,** 10 (2016). https://doi.org/10.1002/cssc.201501228

[2] A. Kojima, K. Teshima, Y. Shirai, and T. Miyasaka, Journal of American Chemical Society, **131,** 6050 (2009). https://doi.org/10.1021/ja809598r
[3] M.A. Green, A. Ho-Baillie, and H.J. Snaith, Nature Photonics, **8,** 506 (2014). https://doi.org/10.1038/nphoton.2014.134
[4] Z. Qu, F. Ma, Y. Zhao, X. Chu, S. Yu, and J. You, Chinese Physics Letters, **38,** 107801 (2021). https://doi.org/10.1088/0256-307X/38/10/107801
[5] B. Ai, Z. Fan, and Z.J. Wong, Microsystems & Nanoengineering, **8**, 5 (2022). https://doi.org/10.1038/s41378-021-00334-2
[6] Z.N. Jahanbakhshi, Z.M. Borhani, and M.R. Nateghi, Thin Solid Films, **671,** 139 (2019). https://doi.org/10.1016/j.tsf.2018.12.029
[7] E. Danladi, M. Kashif, A. Ichoja, and B.B. Ayiya, Transactions of Tianjin University, **28**(5), (2022). https://doi.org/10.1007/s12209-022-00343-w
[8] G. Pindolia, S. M. Shinde, and P.K. Jha, Solar Energy, **236,** 802 (2022). https://doi.org/10.1016/j.solener.2022.03.053
[9] W. Ke, and M.G. Kanatzidis, Nature Communications, **10,** 965 (2019). https://doi.org/10.1038/s41467-019-08918-3
[10] N.K. Noel, S.D. Stranks, A. Abate, C. Wehrenfennig, S. Guarnera, A.A. Haghighirad, A. Sadhanala, G.E. Eperon, S.K. Pathak, M.B. Johnston, A. Petrozza, L.M. Herz, and H.J. Snaith, Energy & Environmental Science, **7,** 3061 (2014). https://doi.org/10.1039/C4EE01076K
[11] M. Roknuzzaman, K. Ostrikov, H. Wang, A. Du, and T. Tesfamichael, Scientific Reports, **7,** 14025 (2017). https://doi.org/10.1038/s41598-017-13172-y
[12] D. Sabba, H.K. Mulmudi, R.R. Prabhakar, T. Krishnamoorthy, T. Baikie, P.P. Boix, S. Mhaisalkar, and N. Mathews, Journal of Physical Chemistry C, **119,** 1763–1767 (2015). https://doi.org/10.1021/jp5126624
[13] M.H. Kumar, S. Dharani, W.L. Leong, P.P. Boix, R.R. Prabhakar, T. Baikie, C. Shi, H. Ding, R. Ramesh, M. Asta, M. Graetzel, S.G. Mhaisalkar, and N. Mathews, Advanced Materials, **26,** 7122–7127 (2014). https://doi.org/10.1002/adma.201401991
[14] B. Wu, Y. Zhou, G. Xing, Q. Xu, H.F. Garces, A. Solanki, T.W. Goh, N.P. Padture, and T.C. Sum, Advanced Functional Materials, **27,** 1604818 (2017). https://doi.org/10.1002/adfm.201604818
[15] H. Wei, P. Qiu, Y.E. Li, Y. He, M. Peng, X. Zheng, and X. Liu, Ceramics International, **48**(5), 5876 (2021). https://doi.org/10.1016/j.ceramint.2021.11.184
[16] M. Chen, M.G. Ju, H.F. Garces, A.D. Carl, L.K. Ono, Z. Hawash, Y. Zhang, T. Shen, Y. Qi, R.L. Grimm, D. Pacifici, X.C. Zeng, Y. Zhou, and N.P. Padture, Nature Communications, **10,** 16 (2019). https://doi.org/10.1038/s41467-018-07951-y
[17] M.G. Ju, M. Chen, Y. Zhou, J. Dai, L. Ma, N.P. Padture, and X.C. Zeng, Joule, **2,** 1231 (2018). https://doi.org/10.1016/j.joule.2018.04.026
[18] T. Leijtens, G.E. Eperon, N.K. Noel, S.N. Habisreutinger, A. Petrozza, and H.J. Snaith, Advanced Energy Materials, **5,** 1500963 (2015). https://doi.org/10.1002/aenm.201500963
[19] O.A. Muhammed, E. Danladi, P.H. Boduku, J. Tasiu, M.S. Ahmad, and N. Usman, East European Journal of Physics, **2**, 146 (2021). https://doi.org/10.26565/2312-4334-2021-2-12
[20] E. Danladi, M.Y. Onimisi, S. Garba, R.U. Ugbe, J.A. Owolabi, O.O. Ige, G.J. Ibeh, and A.O. Muhammed, Journal of the Nigerian Society of Physical Sciences, **1,** 72 (2019). https://doi.org/10.46481/jnsps.2019.13
[21] A. Tara, V. Bharti, S. Sharma, and R. Gupta, Optical Materials, **128**, 112403 (2022). https://doi.org/10.1016/j.optmat.2022.112403
[22] H. Pan, X. Zhao, X. Gong, H. Li, N.H. Ladi, X.L. Zhang, W. Huang, S. Ahmad, L. Ding, Y. Shen, M. Wang, and Y. Fu, Materials Horizons, **7,** 2276 (2020). https://doi.org/10.1039/D0MH00586J
[23] N.S.N. M. Alias, F. Arith, A.N. Mustafa, M.M. Ismail, N.F. Azmi, and M.S. Saidon, Journal of Engineering and Technological Sciences, **54**(4), 220409 (2022). https://doi.org/10.5614/j.eng.technol.sci.2022.54.4.9
[24] M.F.M. Noh, C.H. Teh, R. Daik, E.L. Lim, C.C. Yap, M.A. Ibrahim, N.A. Ludin, A.R.B.M. Yusoff, J. Jang, and M.A.M. Teridi, Journal of Materials Chemistry C, **6,** 682 (2018). https://doi.org/10.1039/C7TC04649A
[25] H. Sabbah, Materials, **15,** 3229 (2022). https://doi.org/10.3390/ma15093229
[26] N. Singh, A. Agarwal, and M. Agarwal, Superlattices and Microstructures, **149,** 106750 (2021). https://doi.org/10.1016/j.spmi.2020.106750
[27] S.M. Seyed-Talebi, and J. Beheshtian, International Journal of Energy and Power Engineering, **15**(6), 252 (2021).
[28] K. Chakraborty, M.G. Choudhury, and S. Paul, Solar Energy, **194**, 886 (2019). https://doi.org/10.1016/j.solener.2019.11.005
[29] F. Hao, C.C. Stoumpos, D.H. Cao, R.P. Chang, and M.G. Kanatzidis, Nature Photonics, **8**(6), 489 (2014). https://doi.org/10.1038/nphoton.2014.82
[30] W. Ning, F. Wang, B. Wu, J. Lu, Z. Yan, X. Liu, Y. Tao, J.M. Liu, W. Huang, M. Fahlman, and L. Hultman, Advanced Materials, **30**(20), 1706246 (2018). http://dx.doi.org/10.1002/adma.201706246
[31] S.Z. Haider, H. Anwar, and M. Wang, Semiconductor Science and Technology, **33**(3), 035001 (2018). https://doi.org/10.1088/1361-6641/aaa596
[32] C.M. Wolff, P. Caprioglio, M. Stolterfoht, and D. Neher, Advanced Materials, **31**(52), 1902762 (2019). http://dx.doi.org/10.1002/adma.201902762
[33] M.I. Hossain, F.H. Alharbi, and N. Tabet, Solar Energy, **120**, 370 (2015). https://doi.org/10.1016/j.solener.2015.07.040
[34] C.S. Solanki, Solar Photovoltaics: Fundamentals, Technologies and Applications, (PHI Learning Pvt. Ltd., New Delhi, 2015).
[35] F. Anwar, R. Mahbub, S.S. Satter, and S.M. Ullah, International Journal of Photoenergy, Article ID 9846310, (2017). https://doi.org/10.1155/2017/9846310
[36] J.P. Correa-Baena, M. Anaya, G. Lozano, W. Tress, K. Domanski, M. Saliba, T. Matsui, T.J. Jacobsson, M.E. Calvo, A. Abate, M. Grätzel, H. Míguez, and A. Hagfeldt, Advanced Materials, **28**(5031), 7 (2016). https://doi.org/10.1002/adma.201600624
[37] A. Mahmood, T. Munir, M. Fakhar-e-Alam, M. Atif, K. Shazad, K.S. Alimgeer, T.G. Nguyen H. Ahmad, and S. Ahmad, Journal of King Saud University-Science, **34**(2), 101796, (2022). https://doi.org/10.1016/j.jksus.2021.101796
[38] E. Danladi**,** M. Kashif, T.O. Daniel, C.U. Achem, M. Alpha, and M. Gyan, East European Journal of Physics, **3**, 19 (2022). https://doi.org/10.26565/2312-4334-2022-3-03

ЧИСЕЛЬНЕ ДОСЛІДЖЕННЯ 25,459% ЛЕГОВАНОГО НЕОРГАНІЧНОГО БЕЗСВИНЦЕВОГО СОНЯЧНОГО ЕЛЕМЕНТА НА ОСНОВІ ПЕРОВСКІТУ $CsSnGeI_3$ ШЛЯХОМ СИМУЛЯЦІЇ ПРИСТРОЮ

Мухаммед О. Абдулмалік[a], Елі Данладі[b], Ріта С. Обасі[c], Філібус М. Гюк[d], Френсіс У. Саліфу[a], Сулейман Магаджі[e], Анселем С. Егбуга[f], Даніель Томас[d]

[a]Фізичний факультет, Науково-технологічний університет Конфлюенс, Осара, штат Когі, Нігерія
[b]Фізичний факультетФедеральний університет наук про здоров'я, Отукпо, штат Бенуе, Нігерія
[c]Центр розвитку супутникових технологій NASRDA, Абуджа, Нігерія
[d]Фізичний факультет, Університет штату Кадуна, Кадуна, Нігерія
[e]Факультет електроніки та інженерії зв'язку, Нігерійська оборонна академія, Кадуна, Нігерія
[f]Операційний підрозділ, Starsight Energy, Нігерія

Токсичний свинцевий компонент, а також дорогий і менш стабільний spiro-OMeTAD у перовскітних сонячних елементах (PSC) створюють велику перешкоду для їх комерційної життєздатності. У цьому дослідженні було запропоновано та реалізовано обчислювальний підхід до моделювання та симуляції всіх неорганічних перовскітних сонячних елементів на основі цезію олова-германію ($CsSnGeI_3$) за допомогою інструменту імітатора ємності сонячних елементів (SCAPS–1D). Допований алюмінієм оксид цинку (ZnO:Al) і йодид міді (CuI) використовувалися як транспортні шари електронів і дірок (ETL і HTL) відповідно. Початковий пристрій без будь-якої оптимізації дав ефективність перетворення потужності (PCE) 24,826%, коефіцієнт заповнення (FF) 86,336%, щільність струму короткого замикання (J_{sc}) 26,174 мА/см^2 і напругу холостого ходу (V_{oc}) 1,099 В. При зміні вищезазначених параметрів індивідуально, зберігаючи інші незмінними, оптимальні значення становлять 1000 нм для товщини поглинача, 10^{14} см$^{-3}$ для щільності дефектів шару поглинача, 50 нм для товщини ETL, 10^{17} см$^{-3}$ для концентрації легування ETL і 260 K для температури . Моделювання з цими оптимізованими значеннями призводить до PCE 25,459%, V_{oc} 1,145 В, J_{sc} 25,241 мА/см^2 і FF 88,060%. Ці результати вказують на те, що $CsSnGeI_3$ є життєздатним альтернативним поглинаючим шаром для використання в конструкції перовскітного сонячного елемента з високим PCE.

Ключові слова: перовскітні сонячні елементи, SCAPS–1D, $CsSnGeI_3$, дірковий транспортний матеріал, електротранспортний матеріал